Gas concentration measurement by optical similitude absorption spectroscopy: methodology and experimental demonstration

Christophe Anselmo, Jean-Yves Welschinger, Jean-Pierre Cariou, Alain Miffre, Patrick Rairoux

Gas concentration measurement by optical similitude absorption spectroscopy: methodology and experimental demonstration

Christophe Anselmo,[1] Jean-Yves Welschinger,[2] Jean-Pierre Cariou,[3] Alain Miffre,[1] and Patrick Rairoux[1,*]

[1]*Institut Lumière Matière, UMR5306 Université Lyon 1-CNRS, Université de Lyon, 10 rue Ada Byron, 69622 Villeurbanne, France*
[2]*Institut Camille Jordan, UMR 5208 Université Lyon 1-CNRS, Université de Lyon, 69622 Villeurbanne cedex, France*
[3]*Leosphere France, 14-16 rue Jean Rostand, 91400 Orsay, France*
[*]*patrick.rairoux@univ-lyon1.fr*

Abstract: We propose a new methodology to measure gas concentration by light-absorption spectroscopy when the light source spectrum is larger than the spectral width of one or several molecular gas absorption lines. We named it optical similitude absorption spectroscopy (OSAS), as the gas concentration is derived from a similitude between the light source and the target gas spectra. The main OSAS-novelty lies in the development of a robust inversion methodology, based on the Newton-Raphson algorithm, which allows retrieving the target gas concentration from spectrally-integrated differential light-absorption measurements. As a proof, OSAS is applied in laboratory to the $2\nu_3$ methane absorption band at 1.66 µm with uncertainties revealed by the Allan variance. OSAS has also been applied to non-dispersive infra-red and the optical correlation spectroscopy arrangements. This all-optics gas concentration retrieval does not require the use of a gas calibration cell and opens new tracks to atmospheric gas pollution and greenhouse gases sources monitoring.

OCIS codes: (300.6340) Spectroscopy, infrared; (280.4788) Optical sensing and sensors; (010.0280) Remote sensing and sensors; (280.1120) Air pollution monitoring.

References and links

1. J. Lelieveld, J. S. Evans, M. Fnais, D. Giannadaki, and A. Pozzer, "The contribution of outdoor air pollution sources to premature mortality on a global scale," Nature **525**(7569), 367–371 (2015).
2. T. F. Stocker, D. Qin, G. K. Plattner, M. Tignor, S. K. Allen, J. Boschung, A. Nauels, Y. Xia, B. Bex, and B. M. Midgley, "IPCC, 2013: climate change 2013: the physical science basis. contribution of working group I to the fifth assessment report of the Intergovernmental Panel on Climate Change" (2013).
3. J. Hodgkinson and R. P. Tatam, "Optical gas sensing: a review," Meas. Sci. Technol. **24**(1), 012004 (2013).
4. C. Stephan, M. Alpers, B. Millet, G. Ehret, P. Flamant, and C. Deniel, "MERLIN: a space-based methane monitor," Proc. SPIE **8159**, 815908 (2011).
5. L. Fiorani, S. Santoro, S. Parracino, M. Nuvoli, C. Minopoli, and A. Aiuppa, "Volcanic CO2 detection with a DFM/OPA-based lidar," Opt. Lett. **40**(6), 1034–1036 (2015).
6. P. Rairoux, H. Schillinger, S. Niedermeier, M. Rodriguez, F. Ronneberger, R. Sauerbrey, B. Stein, D. Waite, C. Wedekind, H. Wille, L. Wöste, and C. Ziener, "Remote sensing of the atmosphere using ultrashort laser pulses," Appl. Phys. B. **71**(4), 573–580 (2000).
7. B. L. Fawcett, A. M. Parkes, D. E. Shallcross, and A. J. Orr-Ewing, "Trace detection of methane using continuous wave cavity ring-down spectroscopy at 1.65 µm," Phys. Chem. Chem. Phys. **4**(24), 5960–5965 (2002).
8. G. B. Rieker, F. R. Giorgetta, W. C. Swann, J. Kofler, A. M. Zolot, L. C. Sinclair, E. Baumann, C. Cromer, G. Petron, C. Sweeney, P. P. Tans, I. Coddington, and N. R. Newbury, "Frequency-comb-based remote sensing of greenhouse gases over kilometer air paths," Optica **1**(5), 290 (2014).
9. C. Massie, G. Stewart, G. McGregor, and J. R. Gilchrist, "Design of a portable optical sensor for methane gas detection," Sens. Actuators B Chem. **113**(2), 830–836 (2006).

#262288 Received 14 Apr 2016; revised 24 May 2016; accepted 25 May 2016; published 1 Jun 2016

10. D. J. Hoch, J. Buxmann, H. Sihler, D. Pöhler, C. Zetzsch, and U. Platt, "An instrument for measurements of BrO with LED-based cavity-enhanced differential optical absorption spectroscopy," Atmos. Meas. Tech. **7**(1), 199–214 (2014).
11. A. S. Diba, F. Xie, B. Gross, L. C. Hughes, C. E. Zah, and F. Moshary, "Application of a broadly tunable SG-DBR QCL for multi-species trace gas spectroscopy," Opt. Express **23**(21), 27123–27133 (2015).
12. B. Thomas, G. David, C. Anselmo, J.-P. P. Cariou, A. Miffre, and P. Rairoux, "Remote sensing of atmospheric gases with optical correlation spectroscopy and lidar: First experimental results on water vapor profile measurements," Appl. Phys. B. **113**(2), 265–275 (2013).
13. P. Chambers, E. A. D. Austin, and J. P. Dakin, "Theoretical analysis of a methane gas detection system, using the complementary source modulation method of correlation spectroscopy," Meas. Sci. Technol. **15**(8), 1629–1636 (2004).
14. E. Vargas-Rodríguez and H. N. Rutt, "Design of CO, CO_2 and CH_4 gas sensors based on correlation spectroscopy using a Fabry–Perot interferometer," Sens. Actuators B Chem. **137**(2), 410–419 (2009).
15. B. Thomas, G. David, C. Anselmo, E. Coillet, K. Rieth, A. Miffre, J.-P. Cariou, and P. Rairoux, "Remote sensing of methane with broadband laser and optical correlation spectroscopy on the Q-branch of the $2\nu_3$ band," J. Mol. Spectrosc. **291**, 3–8 (2013).
16. L. S. Rothman, I. E. Gordon, Y. Babikov, A. Barbe, D. Chris Benner, P. F. Bernath, M. Birk, L. Bizzocchi, V. Boudon, L. R. Brown, A. Campargue, K. Chance, E. A. Cohen, L. H. Coudert, V. M. Devi, B. J. Drouin, A. Fayt, J.-M. Flaud, R. R. Gamache, J. J. Harrison, J.-M. Hartmann, C. Hill, J. T. Hodges, D. Jacquemart, A. Jolly, J. Lamouroux, R. J. Le Roy, G. Li, D. A. Long, O. M. Lyulin, C. J. Mackie, S. T. Massie, S. Mikhailenko, H. S. P. Müller, O. V. Naumenko, A. V. Nikitin, J. Orphal, V. Perevalov, A. Perrin, E. R. Polovtseva, C. Richard, M. A. H. Smith, E. Starikova, K. Sung, S. Tashkun, J. Tennyson, G. C. Toon, V. G. Tyuterev, and G. Wagner, "The HITRAN2012 molecular spectroscopic database," J. Quant. Spectrosc. Radiat. Transf. **130**, 4–50 (2013).
17. J. Dakin, H. Edwards, and B. Weigl, "Progress with optical gas sensors using correlation spectroscopy," Sens. Actuators B Chem. **29**(1), 87–93 (1995).
18. W. H. Press, *Numerical Recipes: the Art of Scientific Computing* (Cambridge University, 2007).
19. D. Kaplan and P. Tournois, "Acousto-optic spectral filtering of femtosecond laser pulses," in *Ultrafast Optics IV* (Springer, 2004).
20. Y. Sun, W. Liu, S. Wang, S. Huang, and X. Yu, "Method of sensitivity improving in the non-dispersive infrared gas analysis system," Chin. Opt. Lett. **9**(6), 8–11 (2011).
21. P. Werle, R. Miicke, and F. Slemr, "The limits of signal averaging in atmospheric trace-gas monitoring by tunable diode-laser absorption spectroscopy (TDLAS)," Appl. Phys. B **57**(2), 131–139 (1993).
22. C. L. Korb and C. Y. Weng, "Effective frequency technique for finite spectral bandwidth effects," Appl. Opt. **43**(18), 3747–3751 (2004).

1. Introduction

Light absorption spectroscopy in the Earth's atmosphere has largely contributed to understanding the impact of anthropogenic gas emissions to air pollution and consequently to human health [1] and global warming [2]. However, large uncertainties still remain, which mainly originate from inaccurate evaluations of gas emission sources [2]. Monitoring the emission of gases is indeed difficult to achieve in industrial and urban sites but also in environments presenting poor infrastructures. This concern underscores the need for developing robust and accurate methodologies to assess gas concentrations, which is the context of this work.

A comprehensive review, providing the state-of-the-art techniques on optical gas sensing, can be found in [3]. To monitor atmospheric gases, several monitoring devices have been proposed, based on high resolution spectroscopy [4–8] or non-dispersive absorption spectroscopy [9], either with point source measurement [10] or laser-based stand-off arrangements [11,12], often by applying effective cross-sections for low optical depths [9]. In non-dispersive absorption spectroscopy, the target gas (TG) concentration is evaluated from absorbance measurements which require an absolute calibration of gas concentration. It uses a light source whose spectral width is larger than the TG-absorption spectral linewidths. The optical correlation spectroscopy technique [13,14] is a particular arrangement of non-dispersive absorption spectroscopy in which a reference cell, filled with the TG, acts as a spectral filter. For field or airborne applications, it should then be limited to non-explosive gases, different from methane for example. However, non-dispersive absorption spectroscopy measurements interestingly remain accurate even for large variations of atmospheric pressure (1000-100 hPa) and temperature (230-500 K) [15], as required for identifying TG emitters from combustion or explosive sources.

#262288 Received 14 Apr 2016; revised 24 May 2016; accepted 25 May 2016; published 1 Jun 2016

To retrieve gas concentration from non-dispersive differential absorption measurements without the use of a standard gas calibration procedure, we here introduce a new concentration retrieval methodology. We have named it Optical Similitude Absorption Spectroscopy (OSAS), as the gas concentration is derived by achieving a similitude between the light source and the target gas spectra. Basically, OSAS can be described in the statistical theory as a non-zero similitude or covariance operator between the emitted power spectrum of the light source and the TG-absorption spectrum. Since OSAS deals with spectrally-integrated measurements, the standard inversion of the monochromatic Beer-Lambert law cannot be applied. Hence, a quantitative evaluation of the TG-concentration from OSAS-measurements is a priori not straightforward. However, TG-concentration is here determined by applying a new robust inversion methodology, based on the Newton-Raphson iterative algorithm. In this study, the OSAS-methodology is proved in laboratory by determining methane gas concentration from non-dispersive light absorption, by using only optical compounds, which is new to our knowledge. Hence we here show that, starting from the spectrum of the OSAS opto-electronic detection efficiency, the iterative Newton-Raphson algorithm can be applied to such differential light absorption measurements.

The paper is organized as follows. In Section 2, the formalism of the OSAS-methodology is presented, by starting from the spectrally-integrated Beer-Lambert law. To achieve a spectral similitude with the TG-absorption spectrum, amplitude modulations of a broadband spectral light source and the methane $2\nu_3$ ro-vibrational absorption band [16] are considered. A study on the amplitude modulation spectral characteristics (central wavelength and spectral width) and their consequences on the OSAS-sensitivity is then presented. Section 3 is dedicated to the experimental proof of the OSAS-methodology in laboratory by evaluating methane gas concentrations in a 1-meter gas cell. To show that the OSAS-methodology can be applied with different amplitude modulation techniques, three different optical arrangements (Acousto-Optic Programmable Dispersive Filter (AOPDF), interference filters as in NDIR, gas absorption cell as in Optical Correlation Spectroscopy (OCS)), are then considered to perform the light source amplitude modulation. By applying our OSAS-inversion algorithm, all three arrangements provide consistent methane gas concentrations within respective error bars. This new methodology hence appears as a robust TG-concentration retrieval procedure when dealing with non-dispersive absorption spectroscopy. The paper ends with a conclusion and proposes outlooks of this work, emphasizing possible applications of the OSAS-methodology coupled with point source measurements and laser remote sensing, to monitor air pollution and to identify greenhouse gas emission sources.

2. OSAS methodology

2.1 Principle

In the OSAS-methodology, the power spectral density (PSD) of a broadband light source (i.e. broader than the spectral width of one or several molecular absorption lines), is tuned or spectrally shaped to be similar with the TG-gas absorption spectrum (the active channel), while a second PSD is set or shaped in a less absorbing spectral region (the reference channel). Ideally, both PSD must be carefully set to ensure that no interfering species absorbs in their respective spectral ranges [3]. The OSAS-principle is shown in more details in Fig. 1 when considering methane in its $2\nu_3$ absorption band. The active channel $P_{0;1}(\lambda)$, which overlaps a high density of absorption lines, undergoes light absorption along the optical path, while the reference channel $P_{0;2}(\lambda)$ experiences a lower light extinction. Hence, two different signals, S_1 and S_2, are detected after light absorption. In Fig. 1, $\eta(\lambda)$ is the spectrum of the opto-electronic efficiency of the detection part of the set-up. This figure is derived from laboratory measurements to be detailed and discussed in Section 3.

#262288 Received 14 Apr 2016; revised 24 May 2016; accepted 25 May 2016; published 1 Jun 2016

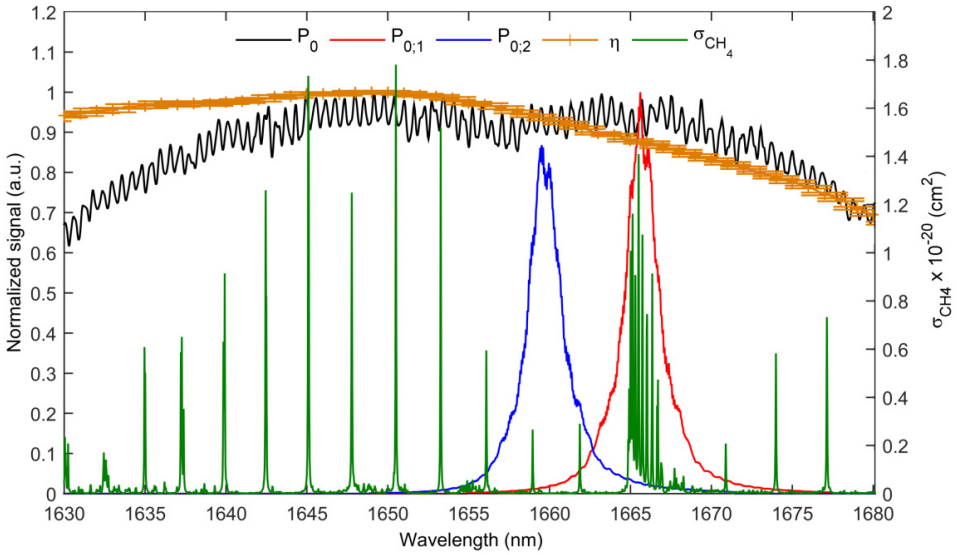

Fig. 1. The OSAS-principle applied to the methane gas. The power spectral density (PSD, black curve) of a broadband light source is spectrally shaped to enfold (red curve) or not (blue curve) the methane absorption cross-section spectrum $\sigma_{CH4}(\lambda)$. The $2\nu_3$ absorption band is here considered (green lines), calculated from HITRAN 2012 database [16] for T = 294 K, p = 1013.25 mbar and air-broadening; a Voigt profile is used to model the line-shape. $\eta(\lambda)$ is the spectrum of the opto-electronic efficiency of the OSAS detection part (orange curve).

Following the Beer-Lambert law, the detected optical signals S_i (i = 1, 2) can be expressed as follows in the absence of interfering species:

$$S_i = K \int_{\Delta\lambda} P_{0;i}(\lambda) T_{TG}(\lambda) \eta(\lambda)\, d\lambda \qquad (1)$$

where $T_{TG}(\lambda) = \exp(-\sigma_{TG}(\lambda) N \ell)$ is the optical transmission of the TG, N is the gas concentration, $\sigma_{TG}(\lambda)$ the TG absorption cross-section at wavelength λ and ℓ is the optical path length. The integral is considered to be taken over the wavelength range $\Delta\lambda$, extending over $P_{0;1}(\lambda)$ and $P_{0;2}(\lambda)$. K is an opto-electronic conversion factor assumed to be achromatic and constant during the measurements. The spectral shape or the position of $P_{0;i}(\lambda)$ can be modified by tuning the light source or by applying several modulation techniques, such as a gas correlation cell with pressure modulation [17] or a Fabry-Perot interferometer [14]. In the present work, a broadband light source $P_0(\lambda)$ is spectrally shaped by applying active or passive optical filters or by using a gas absorption cell. In these cases, the expression of $P_{0;i}(\lambda)$ can be decomposed as follows:

$$P_{0;i}(\lambda) = P_0(\lambda) \cdot M_i(\lambda) \qquad (2)$$

where the amplitude modulation (AM) functions $M_i(\lambda)$ depend on the amplitude modulator device, as detailed in Section 3.

2.2 Target gas concentration retrieval

We here propose a new TG-concentration retrieval procedure from non-dispersive differential absorption signal. As Eq. (1) is non-linear with N, the traditional approach is to linearize this equation [9] and to consider the S_1/S_2-ratio between the measured signals [3]. In this paper, we still retrieve the concentration from the S_1/S_2-ratio but we propose a new TG-concentration retrieval procedure, which is valid whatever the optical depth. It is based on a root-finding algorithm, such as the iterative Newton-Raphson algorithm, which is adequate

#262288 Received 14 Apr 2016; revised 24 May 2016; accepted 25 May 2016; published 1 Jun 2016

for solving non-linear problems [18]. We therefore introduce the following function g defined by the cross-product:

$$g(x) = S_2 f_1(x) - S_1 f_2(x) \tag{3}$$

whose x-variable is related to the TG-concentration while f_i is a function modeling the detected signal defined as:

$$f_i(x) = \int_{\Delta\lambda} P_{0;i}(\lambda) \exp\left(-x\sigma(\lambda)\ell\right)\eta(\lambda)\, d\lambda \tag{4}$$

Compared with Eq. (1), K does not appear in the expression of f_i since, as explained above, K is achromatic over $\Delta\lambda$ and constant during signal measurement. Interestingly, the x-variable corresponds to N when the S_1/S_2-ratio is equal to the f_1/f_2-ratio. As a result, the gas concentration N appears as the first zero of the g-function which can be retrieved by applying a root-finding algorithm, such as the iterative Newton-Raphson algorithm. At the n^{th}-iteration, starting from $x_0 = 0$, the solution of this algorithm is given by $x_{n+1} = x_n - g(x_n)/g'(x_n)$. A unique solution is ensured when $g' < 0$, $g'' > 0$ and N belongs to $[0; x_{max}]$, where x_{max} is the first zero of the f_1/f_2 first derivative. These mathematical conditions reflect the non-linearity of the measured signals S_i when increasing the gas concentration N, as a result of the Beer-Lambert law. The x_{max}-value depends on the experimental set-up but is very high, above 10^{28} $\#.m^{-3}$ for the three experimental configurations presented in Section 3. To highlight the convergence of the inversion algorithm in the case of a high methane optical depth, the g-function is displayed in Fig. 2(a). The numerical relative error is below 10^{-12} after only n = 5 iterations and reaches the computation limit (about 10^{-16}) after only 7 iterations (see Fig. 2(b)).As a result, the gas concentration can be retrieved if the f_i-function can be calculated, which requires knowledge of the spectral dependence of Eq. (1) variables, and assuming that they remain stable over time. Hence, OSAS-methodology does not require the use of a gas calibration procedure, as usually presented in the literature.

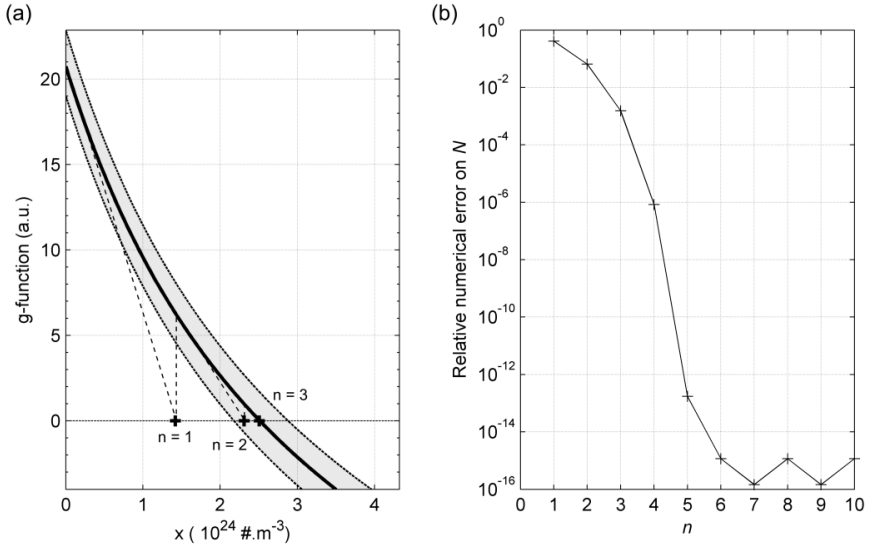

Fig. 2. a) The iterative Newton-Raphson algorithm applied to a methane concentration of $N = 2.5.10^{24}$ $\#.m^{-3}$ (black line). Its convergence is shown with successive iterations (labeled by the iteration number n) while the grey area represents the variation of g when considering ± 2% statistical errors on S_i. b) Relative numerical error on N as a function of the iteration number n.

#262288 Received 14 Apr 2016; revised 24 May 2016; accepted 25 May 2016; published 1 Jun 2016

When considering the uncertainties affecting the measured signals S_i, the root-finding algorithm converges to the target gas concentration with an uncertainty that depends on the statistical uncertainties and biases on the measured signals S_i as displayed in grey in Fig. 2(a). To provide an order of magnitude on the knowledge and stability requirements on P_0 and η, we considered the rather pessimistic case where a 2%-uncertainty is affecting the measured signals. Such a 2%-relative error on S_i corresponds to a 3.9 nm shift in the central wavelength (CWL) of the PSD (1.3 nm in its spectral width), or a 1.8 nm shift in the opto-electronic efficiency spectrum, or a 0.4 nm shift in the CWL of the M_1-modulation (6.1 nm for the M_2-modulation). The corresponding relative error on the gas concentration for a path-integrated concentration of 10^5 ppm.m is 23% for the CWL of the PSD ($5.10^{-3\%}$ for its spectral width, 0.8% for a shift in η and 16% for the two modulation functions). Therefore, CWL shifts in P_0 and M_i in the nanometre range are acceptable. When the 2%-relative error on S_i are of statistical origin, the relative error on the gas concentration is 24%. Moreover, from an experimental point of view, the stability of the measurements with time can be indirectly verified by evaluating the Allan variance, as explained by Werle et al. [21].

2.3 Normalized weighted transmission

OSAS-measurements depend on the TG-absorption spectrum as well as on the chosen spectral properties of the AM functions. In the absence of interfering species, these dependencies can be studied by evaluating the normalized weighted transmission $T_w(\lambda_i)$ of a TG-sample cell, which is defined as follows:

$$T_w(\lambda_i) = \frac{\int_{\Delta\lambda} P_0(\lambda) M(\lambda_i, \lambda) T_{TG}(\lambda) \eta(\lambda)\, d\lambda}{\int_{\Delta\lambda} P_0(\lambda) M(\lambda_i, \lambda) \eta(\lambda)\, d\lambda} \tag{5}$$

where the spectra $P_0(\lambda)$ and $\eta(\lambda)$ are presented in Fig. 1. The AM-function $M(\lambda_i,\lambda)$ simulates a modulation function centered at wavelength λ_i, with a Lorentzian shape function that carefully fits with the AM-experimental spectra presented in Fig. 1 (R^2 = 0.98). The methane transmission $T_{TG}(\lambda)$ is computed from the TG-cross section spectrum $\sigma_{TG}(\lambda)$ by using a path-integrated concentration *Nl* set to 1.10^4 ppm.m, using the HITRAN 2012 database [16] in the same spectral range as in Fig. 1. For that, air-broadening at laboratory temperature and pressure (T = 294 K, P = 1013.25 mbar) is considered in the individual Voigt's line profiles. The normalized transmission $T_w(\lambda_i)$ is shown in Fig. 3 for methane in the 1630-1680 nm range. $T_w(\lambda_i)$ reaches a minimum at 1665.6 nm in the Q-branch. Local maxima are obtained at a central wavelength (CWL) of λ_i = 1660.0 nm, 1630 nm and 1672.3 nm due to the decreasing number of strong methane absorption lines. The influence of the spectral width $\delta\lambda$ of the modulation on $T_w(\lambda_i)$ is also shown in Fig. 3 by considering $\delta\lambda$ = 2.5 nm and $\delta\lambda$ = 5 nm. As expected, the transmission is increasing in the center of the Q-branch when $\delta\lambda$ is increased. Moreover, $T_w(\lambda_i)$ extrema positions are slightly shifted. In complement, the role of interfering gas molecules has been addressed by considering water vapor, carbon dioxide or ethane whose absorption lines lie in the same spectral range as methane. Such calculations however show that these molecules barely affect the normalized transmission $T_w(\lambda_i)$ in the ‰ range even at high methane concentrations, as considered in this study. These results will be used in Section 3 to set the AM-functions which are required to apply the OSAS-methodology. The position of the M_2-modulation function will affect the relative error on the TG-concentration, as shown below.

#262288 Received 14 Apr 2016; revised 24 May 2016; accepted 25 May 2016; published 1 Jun 2016

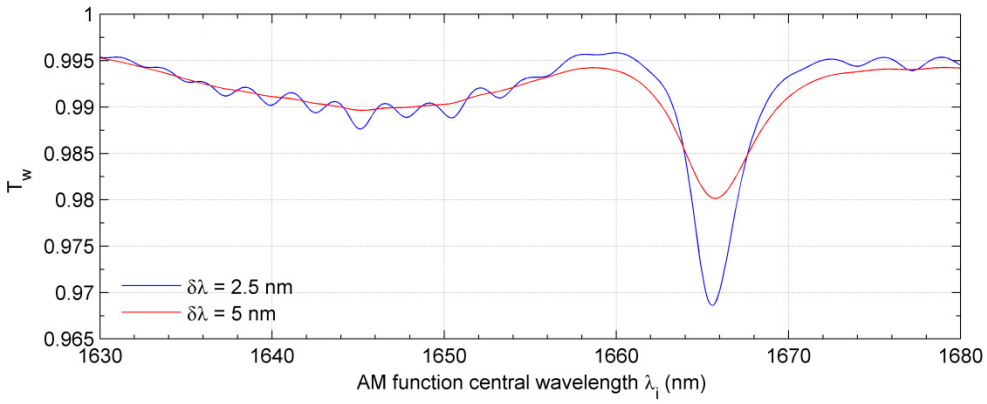

Fig. 3. Normalized weighted transmission $T_w(\lambda_i)$ as a function of the central wavelength λ_i and the amplitude modulation function $M(\lambda_i, \lambda)$, as defined in Eq. (5). Two different modulation spectral widths are considered ($\delta\lambda$ = 2.5 nm, blue curve; $\delta\lambda$ = 5 nm, red curve) in the case study of a path-integrated concentration of 10^4 ppm.m of methane.

3. Experimental set-up

The experimental set-up for applying the OSAS-methodology is shown in Fig. 4. A Superluminescent Light Emitting Diode (SLED, DL-BZ1-CS65M5A from Denselight), emitting at 1650 nm wavelength, is used as the broadband light source with a spectral width of 65 nm (FWHM), to cover a large part of the methane gas absorption spectrum in its $2\nu_3$ absorption band. This light source is pulsed at a 1 kHz pulse repetition rate (20 µs pulse duration) to carry out experiments with an AOPDF in Section 3.1. Light coupling is ensured with a SMF-28 fiber having a 10 µm mode field diameter whose output is collimated with a 10x-microscope objective. The SLED broadband PSD is shown in Fig. 1 between 1630 and 1680 nm. Spectral ripples are related to the SLED coupling with the single mode fiber. A broadband polarizing beam splitter cube sets the p-polarization of the light. Amplitude modulations are applied through three different modulation techniques (I, II and III) to be detailed below. The measurement gas cell (1 meter long) is positioned after the amplitude modulator, but could have been set before [12], since the spectral transmission of the gas cell is constant over the considered spectral range. The gas cell is filled with a mixture of CH_4-clean air and N_2 buffer gas and the gas partial pressures are monitored with a Capacitron (DM21). Gas fluxes are not considered here because it is beyond the scope of this study to achieve a field instrument. The S_i-signals, measured with an Avalanche Photo-Diode (Laser Components, LCIA-200-10) are sampled with a transient recorder (Licel, 14 bits, 20 MHz sample rate), averaged over 1 second and the electronic offset is corrected. The measurement of $P_{0;i}(\lambda)$ is achieved with an intensity and frequency-calibrated spectrograph (ANDOR Shamerock SR-750) using the removable mirror shown in Fig. 4. In this way, any supplementary modulation induced by semi-transparent mirror or polarizing beam splitter is avoided. To ensure that Eq. (1) can be applied, we also verified that the detector and the spectrograph operated in the linear regime, by using calibrated grey filters. For each method, the weighted transmission are: for setup-I, $T_W(\lambda_1) = 0.964$ and $T_W(\lambda_2) = 0.996$; for setup-II, $T_W(\lambda_1) = 0.986$ and $T_W(\lambda_2) = 0.994$; for setup-III: $T_W(\lambda_1) = 0.975$ and $T_W(\lambda_2) = 0.997$.

#262288 Received 14 Apr 2016; revised 24 May 2016; accepted 25 May 2016; published 1 Jun 2016

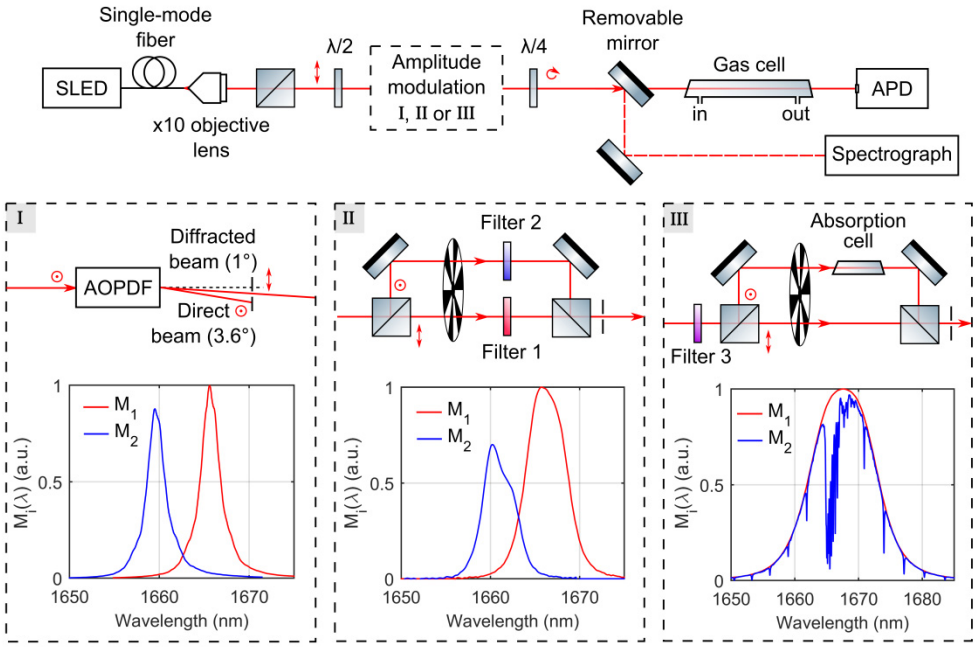

Fig. 4. Scheme of the experimental set-up. The SLED broadband PSD is shaped by an amplitude modulator generating the $M_i(\lambda)$ function, either I or II or III. The S_i-signals are measured with an Avalanche Photo-Diode (APD) after passing through a 1-meter-long gas cell. A removable mirror is added on the optical path for spectral characterizations. A quarter waveplate is used to avoid biases induced by the polarization dependent spectrograph grating efficiency. Each amplitude modulator is described in subsection 3.1, 3.2 and 3.3.

3.1 AOPDF

As shown in the insert I of Fig. 4, the amplitude modulation of the broadband light source can be achieved by using the AOPDF as an active modulator (Dazzler-HR-1000-1650 from Fastlite) to generate versatile $M_i(\lambda)$ functions on the 1°-diffracted beam as presented in Fig. 4(I). AOPDF is frequently used with chirped femtosecond laser [19]. Its maximal transmission and spectral rejection respectively reach 0.6 and 2.10^{-4}. To match the AOPDF polarization specification, a half wave-plate (see Fig. 4) is inserted on the optical pathway. Using the 1 kHz repetition rate of the light source, each light pulse can be alternately - without dead time - adjusted to the active $M_1(\lambda_1, \lambda)$ or to the reference $M_2(\lambda_2, \lambda)$ AM-function. The remaining 3.6°-beam outgoing from the AOPDF is not used here. Examples of the resulting $P_{0;1}(\lambda)$ and $P_{0;2}(\lambda)$ spectra are presented in Fig. 1, for λ_1 = 1666 nm, λ_2 = 1660 nm, with $\delta\lambda$ = 2.5 nm for both modulations. This spectral width of 2.5 nm was the smallest experimental value that could be achieved with our apparatus. The broadband PSD $P_{0;1}(\lambda)$ obtained in Fig. 1 corresponds to an AM-function that effectively overlaps the Q-branch of the methane $2\nu_3$ absorption band, hence addressing the similitude between the $P_{0;1}(\lambda)$ and the TG-absorption spectra. OSAS-measurements are performed in Section 4.3 by using these spectral settings.

3.2 Passive filters

The second modulation technique relies on passive filters as shown in Fig. 4(II) with its related modulation function $M_i(\lambda)$. The two interference filters were designed, in agreement with Section 2.3, to exhibit a transmission FWHM bandwidth of 5.07 nm (respectively 4.04 nm) centered at a CWL of 1666.31 nm (respectively 1660.99 nm). The half waveplate, set before the amplitude modulator, balances the energy between the active (λ_1 = 1666.31 nm)

#262288 Received 14 Apr 2016; revised 24 May 2016; accepted 25 May 2016; published 1 Jun 2016

and the reference (λ_2 = 1660.99 nm) channel. For selecting one channel at a time, a mechanical chopper is implemented and rotated at a 500 Hz frequency which then triggers the SLED pulse. Delays are adjusted so that the SLED alternately emits pulses to the active channel and to the reference channel without cross-talk. Afterwards, the two optical paths are recombined with a polarizing beam splitter cube. For experimental versatility, a chopper is used instead of a conventional filter wheel [20] that may simplify the set-up.

3.3 Absorption cell

The third amplitude modulation technique relies on a gas absorption cell, as presented in Fig. 4(III). The AM-function is here achieved by inserting a 10 cm-sealed methane gas cell, filled with 1500 Torr of pure methane on the optical pathway of the reference channel. It is shown in Fig. 4(III). As the light propagates through this absorption cell, it undergoes the characteristic TG-absorption spectrum, in contrary to the other light pathway, corresponding to the active channel, where no gas cell or optical compound is inserted. Both pathways are recombined with a polarizing beam splitter cube, before entering the 1 m-measurement gas cell. To increase the relative transmission between both channels, the bandwidth of the broadband light source is reduced by inserting an optical filter (Filter 3) before the polarizing beam splitter cube. The AM-functions defined in Eq. (2) then express as: $M_1(\lambda) = T_{IF3}(\lambda)$ and $M_2(\lambda) = T_{IF3}(\lambda) \times T_{cell}(\lambda)$ where T_{IF3} is the transmission of the interference filter 3 and T_{cell} is the transmission of the absorption cell, calculated from the HITRAN database by considering self-broadening and Voigt line profiles at the laboratory temperature of 294 K and using the methane pressure of 1500 Torr. The interference filter 3 is centered at a CWL of 1667.62 nm with a FWHM spectral bandwidth $\delta\lambda$ = 11.46 nm.

4. Methane concentration measurements using OSAS-methodology

In this section, methane concentration measurements are reported by applying OSAS based on the novel inversion formalism introduced in Section 2.2. The spectral behavior of the opto-electronic efficiency η is first measured by using the AOPDF. An OSAS verification is then proposed to indirectly check the validity of the measured spectral parameters (i.e. $P_{0;i}(\lambda)$ and $\eta(\lambda)$). Moreover, four different methane concentrations, corresponding to increasing light absorptions, are then evaluated by applying the OSAS-methodology, for each of the above three amplitude modulators. The obtained results are then compared and discussed.

4.1 Opto-electronic efficiency measurement

To evaluate the opto-electronic efficiency $\eta(\lambda)$ introduced in Section 2.1, we used the AOPDF that operates as a monochromator having a spectral resolution of $\delta\lambda$ = 2.5 nm (see Fig. 4(I)). $\eta(\lambda)$ is hence obtained by interpolating $\eta(\lambda_i)$ measurements characterized between 1.6 and 1.7 µm, assuming η is constant over $\delta\lambda$. Hence, we get:

$$\eta(\lambda_i) = \frac{S(\lambda_i)}{\int_{\Delta\lambda} P_{0;i}(\lambda_i, \lambda)\, d\lambda} \tag{6}$$

where $S(\lambda_i)$ is the detected signal in the absence of absorbing species, when the CWL is set to λ_i. $P_{0;i}(\lambda_i,\lambda)$ is the corresponding spectrum simultaneously recorded with the spectrograph by placing a spectrally-calibrated polarizing cube instead of the removable mirror. The CWL λ_i is swept with the AOPDF from 1.6 µm to 1.7 µm with 1 nm steps. The $\eta(\lambda_i)$-values are normalized and shown in Fig. 1. Absolute measurements are not mandatory since the concentration is retrieved from the ratio S_1/S_2 and the calibration constant K does not appear in the retrieved equations. The decrease of $\eta(\lambda)$ in the high wavelength range is in agreement with our InGaAs APD spectral cut-off. Uncertainties on $\eta(\lambda)$ come from the detector shot-noise (see section 4.3). The uncertainty on λ_i is lower than 0.1 nm and hence not reported in

#262288 Received 14 Apr 2016; revised 24 May 2016; accepted 25 May 2016; published 1 Jun 2016

Fig. 1. In the following sections, we assume that this spectral specification of our optical set-up remains stable over time.

4.2 OSAS-verification

In this section, the OSAS-methodology is verified over a broad spectral range of the TG-absorption spectrum based on the measured spectra $P_{0;i}(\lambda)$ and $\eta(\lambda)$ presented in Fig. 1. The OSAS-methodology has been applied by filling the measurement gas cell with a commercial gas mixture of CH_4 and air (1.8% vol. concentration ± 1% relative error), corresponding to a methane gas path-integrated concentration (PIC) of 18000 ppm.m. The AM-function of the active channel $M_1(\lambda_1, \lambda)$ is set at λ_1 = 1666 nm (Section 2.3, Fig. 3). The CWL λ_2 of the reference channel $M_2(\lambda_2, \lambda)$ is swept from 1630 nm to 1680 nm with 1 nm step to retrieve methane PIC as a function of λ_2. Each methane PIC is retrieved by applying the Newton-Raphson inversion algorithm to the differential absorption measurements using the measured value of $\eta(\lambda)$, that of both power spectral densities $P_{0;i}$, and the calculated methane absorption cross section. Figure 5 presents the OSAS-retrieved methane PIC. Errors bars are evaluated by considering statistical errors on S_1 and S_2. Interestingly, on average over all measurements, the relative error remains below 10% (when considering the median). Within error bars, the retrieved PIC are compatible with the expected value of 18000 ppm.m, except when λ_2 is set too close to λ_1 (between 1665 and 1667 nm), as discussed in Section 2.3. The increase in the error bars in Fig. 5 is due to the SNR on S_i and to the CWL of $M_2(\lambda)$, as expected. Indeed, when considering a 1%-relative error on the S_1/S_2-ratio, a 10%-relative error on N is obtained for every λ_2-value of our numerical spectral range (1630-1680 nm), apart from the spectral interval between 1664.5 and 1667 nm, in agreement with the observed strong increase in the error bars. As expected, the OSAS-methodology is not applicable at λ_2 = 1666 nm since $M_1(\lambda) = M_2(\lambda)$.

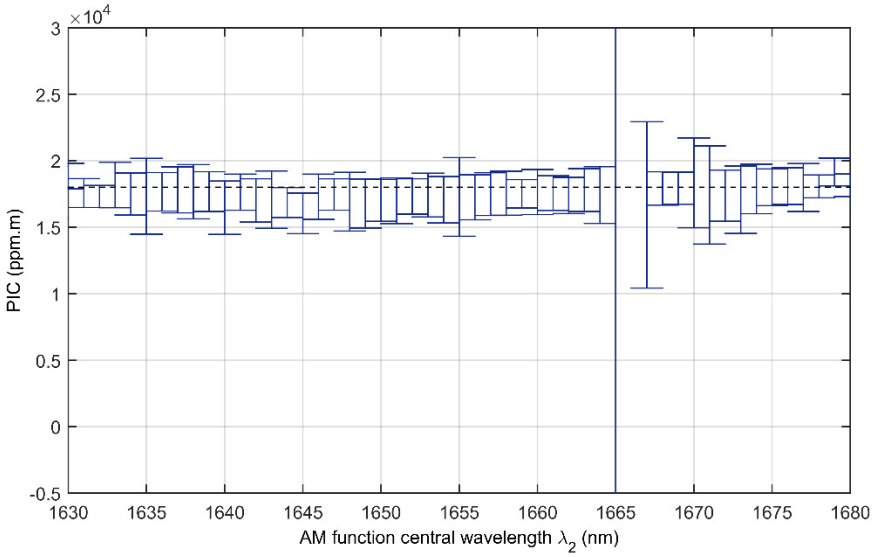

Fig. 5. Methane path-integrated concentrations retrieved from the OSAS-methodology depending on the reference channel AM function central wavelength λ_2. The expected methane PIC is represented in dashed-lines.

4.3 OSAS-measurements

OSAS-measurements are here performed for four different methane PIC (4500, 9000, 13500, 18000 ppm.m), corresponding to increasing light absorptions, by using the three modulation techniques presented in Section 3. The retrieved OSAS PIC are presented in Fig. 6. PIC and

#262288 Received 14 Apr 2016; revised 24 May 2016; accepted 25 May 2016; published 1 Jun 2016

error bars are evaluated by considering the mean value and the standard deviation of the measurements acquired over 20 minutes. In each four methane case study, the measured PIC are comparable within error bars of the respective modulation techniques.

The largest standard deviations are obtained with the absorption cell set-up (Fig. 4(III)) for which the differential absorption is the lowest. These error bars can be further reduced by increasing the absorption in the gas cell or by decreasing the IF3 spectral width (see Fig. 4(III) and Section 3.3). Error bars when using the AOPDF-amplitude modulation (Fig. 4(I)) are larger than those obtained with the IF-amplitude modulation (Fig. 4(II)). This seems contradictory because set-up I provides a greater differential absorption (see Fig. 3) that should induce smaller error on PIC. This loss in sensitivity originates from the AOPDF fast jittering during the AM-generation and from the temperature variation of the SLED PSD. These temperature variations affect all OSAS-measurements causing a detuning of the SLED CWL in the range of ± 0.2 nm. Its consequence on OSAS PIC is highlighted in Fig. 7 by the observed slow oscillation on the retrieved PIC-values (314 ppm.m, with a period of about 10^3 s). The standard deviation of S_1/S_2 as a function of the averaging time τ is shown in the Allan deviation plot in Fig. 7 [21]. As expected, for short signal averaging times, the measurement precision is limited by white noise (following a $\tau^{-1/2}$ trend). It is attributed to statistical AOPDF AM-function jitter and to the detector shot noise. Moreover, the Allan deviation plot exhibits the optimal averaging time around τ = 30 s. At larger τ-values, the standard deviation is increasing, which is related to the previous remark on the SLED temperature change. The abrupt change in the standard deviation at τ = 400 s can be related to inherent - non-strictly periodical - temperature change. Other error contributions from changes in SLED spectral density (e.g. ripples involved in fiber coupling) or variations in opto-electronic efficiency are lower than the previously discussed error sources. When comparing the retrieved methane PIC elaborated from the different amplitude modulators, the OSAS-methodology is found consistent, even if the light and the AOPDF stability affect the precision and the sensitivity of the methodology.

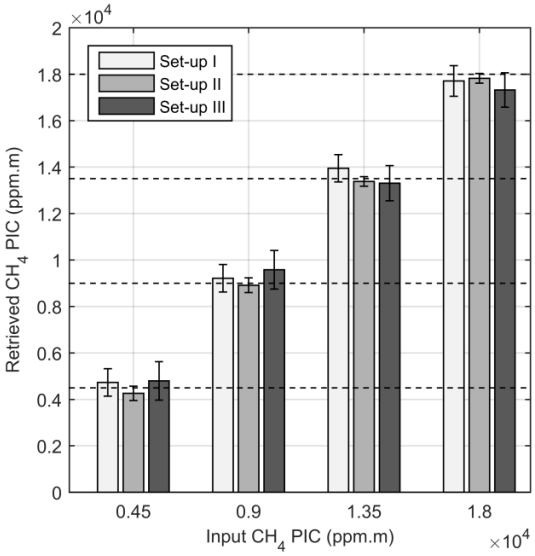

Fig. 6. Methane PIC retrieved by applying different AM-techniques. The expected PIC-values are indicated with the dotted lines for comparison.

#262288 Received 14 Apr 2016; revised 24 May 2016; accepted 25 May 2016; published 1 Jun 2016

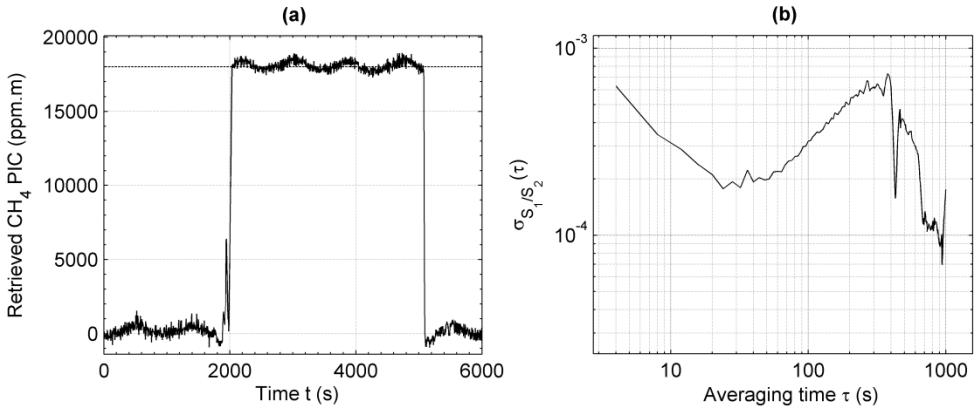

Fig. 7. a) Temporal evolution of methane PIC retrieved with OSAS by using the AOPDF-modulator over 6000 seconds. At time t = 2000 s, the 1-meter-long measurement gas cell buffered with N_2 is filled with a methane-air mixture (1.8% of methane). Then, methane is removed from the gas cell by flushing it with N_2. The stability over time of $P(\lambda)$ and $\eta(\lambda)$ has been directly checked before and after the measurements. b) Allan deviation of the signal ratio S_1/S_2 between t = 2050 s and t = 5050 s.

5. Conclusion and outlooks

In this paper, we present the OSAS, which is a new methodology to evaluate TG-concentrations from spectrally integrated (or non-dispersive) differential absorption measurements. We verify OSAS in laboratory by retrieving methane path integrated concentration. We show that methane PIC is retrieved by applying the Newton-Raphson inversion algorithm on the differential absorption measurements after measuring the optical set-up efficiency and both power spectral densities $P_{0;i}(\lambda)$ and calculating the target gas absorption cross-section. It is also shown that OSAS-methodology can be applied to different light source amplitude modulation techniques (AOPDF, interference filters and absorption gas cell). The spectral fluctuations of the broadband light source should be in the nanometre range, while its amplitude fluctuations will barely affect the TG-concentration retrieval as long as the detected signals are shot-noise limited. Reaching a high sensitivity and a high precision on these measurements was beyond the scope of this work but improvements can be achieved by using a temperature stabilized PSD light source. Moreover, a higher sensitivity can be obtained by considering stronger TG-absorption cross sections as for example for methane, in the ν_3 band at 3.2 μm. Interfering species may be an issue at ambient methane concentrations, but a methane concentration measurement in their presence was beyond of the scope of this study. OSAS could however be considered to carry out several AM-functions covering several TG-absorption bands as a in the standard NDIR [20]. Hence, OSAS appears promising. This work also settles the basements towards the use of the OSAS-methodology to improve DIAL (DIfferential Absorption Lidar) retrievals using broadband laser sources. The remote sensing methodologies relying on effective cross section formalism [22] may also take benefit from the OSAS-concentration inversion methodology to avoid biases related to the light source bandwidth. Moreover, determining quantitative TG-concentrations by applying OSAS can avoid the traditional use of gas calibration concentration procedure but assuming that the spectral specification of the set-up remains stable over time and taking advantage of a comprehensive study on the TG-spectroscopy.

Acknowledgments

The authors thank CIFRE for partly funding this work. We also thank the team of the ILM mechanic workshop for performing precise experimental hardware.

#262288 Received 14 Apr 2016; revised 24 May 2016; accepted 25 May 2016; published 1 Jun 2016